Contents lists available at ScienceDirect

Construction and Building Materials

journal homepage: www.elsevier.com/locate/conbuildmat

High-porosity alkali-activated binders based on glass and aluminium recycling industry waste

A. Maldonado-Alameda [a,b], J. Mañosa [a], T. López-Montero [a,c], R. Catalán-Parra [a], J.M. Chimenos [a,*]

[a] Departament de Ciència de Materials i Química Física, Universitat de Barcelona, 08028 Barcelona, Spain
[b] Fundación Centro Tecnológico de Investigación Multisectorial (CETIM), 15180 Culleredo, A Coruña, Spain
[c] Department of Civil and Environmental Engineering, Universitat Politècnica de Catalunya, 08034 Barcelona, Spain

ARTICLE INFO

ABSTRACT

The potential as alkali-activated precursors of ceramic-stone-porcelain (CSP) and PAVAL, two residues derived from the optical separation of glass cullet and salt slag from secondary aluminium recycling, has been assessed. Alkali-activated CSP and PAVAL binders' formulations were prepared using NaOH 4 M and 6 M as alkaline activator solutions. The effect of the Na_2O/Al_2O_3 ratio and alkaline activator concentration was evaluated from a chemical, physical, mechanical, and environmental perspective. The results revealed the formation of secondary reaction products attributed to the formation of (C,N)-A-S-H gels. It also showed the influence of decreasing Na_2O/Al_2O_3 ratio in the obtained binders, increasing porosity and affecting the mechanical performance. Besides, it was demonstrated that PAVAL acts as a precursor and pore-generator. Finally, the environmental characterisation showed a significant leaching concentration of heavy metal(loid)s such as As, Cr, Mo, Sb, and Se, which decreases with longer curing periods.

1. Introduction

The importance of conserving the environment and the sustainable management of human-generated waste led to seeking new ways to valorise residues currently disposed of in landfills. In this sense, the building and civil engineering fields have incorporated human-generated waste in domestic and industrial areas to produce new construction materials for decades. Moreover, this waste valorisation promotes sustainability by reducing the extraction of natural resources and the space dedicated to landfills and moving towards a low-carbon circular economy.

Waste glass contributes significantly to the increasing volume of urban waste generated worldwide due to ineffective colour sorting methods, high recycling costs, consumerism, and a lack of awareness about recycling benefits in modern societies, [1,2]. Only 21% of 130 million tons of waste glass produced worldwide was recycled in 2018 [3]. Although this material can be reused several times without changing its chemical and physical properties, the amount of recycled non-clear glass is negligible. This fact represents an environmental concern since waste glass will remain stable after being disposed of in landfills

[4]. Therefore, waste glass valorisation in the construction sector has become a priority to reduce deposition, promote circularity, and reduce carbon footprint and natural resources exploitation [5]. The main valorisation route of waste glass in building and civil engineering is focused on developing cement-based materials as supplementary cementitious material (SCM) [6] and ceramic tiles manufacturing [7] due to its pozzolanic properties and composition, respectively. However, a novel research line emerged in the last decades, centring on formulating alkali-activated binders (AABs) using waste glass as a raw material precursor.

AABs arise as a more environmentally sustainable alternative to ordinary Portland cement (OPC) [8,9]. They are obtained from the reaction of a precursor, whose main compound is an aluminosilicate, and an alkaline activator. Thus, AABs offer the possibility of using industrial waste and by-products as raw materials and trying to solve the environmental problem derived from cement production [10]. The most common materials used as precursors in the manufacture of AABs have been metakaolin, fly ash and slag [11]. However, other residues and by-products, such as red mud [12,13], rice husk ash [14] and volcanic ash [15], have also been considered promising precursors candidates. The mechanical behaviour of the obtained AABs depends mainly on the

---

* Corresponding author.
E-mail address: chimenos@ub.edu (J.M. Chimenos).

nature and chemical composition of the precursor. To achieve the desired strength, the ratio of silica and alumina of the materials used for the AABs preparation must be optimal [16]. Likewise, when NaOH or water glass are used as activators, the strength will increase faster, and the achieved ultimate compressive strength should be higher when activators such as Na_2CO_3 and Na_2SO_4 are used [8]. In addition to the raw materials used as precursors and the activators used, the alkali activation process and the mechanical properties of alkaline activated materials will vary depending on the particle size distribution, the temperature, and the liquid-to-solid ratio [11,17].

Previous studies have shown that materials with high alkali and silicate content, such as waste glass, could produce AABs as a precursor [18] or an alkaline activator [19–21] to produce AABs. However, when glass powder is used as a main component in AABs, the generated gels in moisture conditions can leach alkali ions [22], contributing to their structure destabilization [23]. Therefore, since waste glass has a relatively poor alumina content, it is necessary to modify its composition incorporating a certain amount of an Al-rich material to guarantee the formation of the AABs. Few studies in the literature on AABs as a combination of waste glass with other Al-rich precursors have been found. Pascual et al. [4] and Redden and Neithalath [23] studied the possibility of formulating alkali-activated materials by replacing part of the glass powder with metakaolin as an Al-rich source powder to fix alkali ions in the system. Other authors explored the formulation of AABs through the alkali activation of waste glass and red mud [24,25].

This research work proposes, for the first time, the development of AABs through the synergistic combination of two residues rich in silica and aluminium, known as ceramic-stone-porcelain (CSP) and PAVAL, respectively. On the one hand, CSP comes from the soda-lime glass waste recycling process after an optical classification methodology where transparent fragments are separated from opaque ones. In this process, thick glasses such as neck and bottom bottles, or those with labels, are directly rejected, causing the discarded residue contains around 84% of glass, 4% of ceramic and 4% of porcelain [26]. CSP cannot be recycled due to its porcelain content, as the needed temperature to melt the glass is much higher, and its final destination is a landfill. On the other hand, PAVAL is presented as a potential Al-rich material able to compensate for the lack of alumina in the waste glass. PAVAL is the trade name for waste generated during the recycling process of salt slag in the secondary aluminium production process [27]. This recycling process allows recovering free metal, scarified salts, and inert products as PAVAL. The first stage consists of crushing the salt slag blocks and screening the obtained particles as a function of their size. The aluminium is easily recovered since are usually condensed in the thicker fractions and remains defragmented due to its plastic nature. The salts (NaCl and KCl) and metal oxides, which are the finest fragmented particles, are mixed with water to dissolve the former and to obtain PAVAL. Finally, the salts are recovered through steam evaporation and condensation. This residue has a high concentration of aluminium-bearing compounds such as corundum, bayerite, and nordstrandite, among others. Previous studies have shown that a hazardous material such as PAVAL can be used as a precursor and pore-generating agent in AABs formulation [28,29].

The main goal of this research is to formulate AABs through the alkali activation of CSP and PAVAL (AA-CSP/PV) and evaluate the final properties depending on their Na_2O/Al_2O_3 ratio, which varied by using different NaOH solutions at different concentrations as alkaline activators. As a result, four different AAB formulations with different content of CSP and PAVAL have been studied from a chemical, physicomechanical, and environmental perspective.

2. Experimental procedure

2.1. Materials

The CSP sample was provided by the Daniel Rosas S.A company, which collects up to 90 kt·y^{-1} of glass cullet from different municipalities

in the metropolitan area of Barcelona (Spain). This glass cullet is processed and conditioned for subsequent recycling in its treatment plant located in El Prat de Llobregat (Spain). CSP waste consists of glass ($\approx$ 84% wt.), ceramic ($\approx$ 6% wt.), porcelain ($\approx$ 6% wt.), stone ($\approx$ 2% wt.) and other materials such as polymers, paper, and metals ($\approx$ 2% wt.) [26] that are typically present in the waste stream alongside glass cullet. This material fraction (2% wt.) was separated from the glass cullet using an optical sorting process that identifies and separates materials based on their optical properties. It is estimated that 30 kt·y^{-1} are generated in Catalonia (Spain) [26].

The PAVAL was supplied by the BEFESA company. This by-product is generated during the aluminium recycling process when the aluminium oxide is mixed with water to separate it from the salts (NaCl and KCl) through filtration. Around 90 kt·y^{-1} of PAVAL are generated in BEFESA facilities in Valladolid (Spain) [30].

Both CSP and PAVAL (PV) were conditioned to be used as powder precursors rich in silica and alumina, respectively. First, the CSP sample was washed with soap to remove organic matter and other dirt traces. Both materials were then dried in a stove at 105 °C for 24 h to remove the humidity and were subsequently sieved to determine the particle size distribution (PSD) as shown in Fig. 1. Finally, the samples were crushed (only the CSP) and milled to improve their reactivity and obtain two powders of <63-μm particle size. The alkaline activator solutions (NaOH 4 M and 6 M) were prepared using NaOH pearls (PanReac AppliChem, Germany, purity: 98%) dissolved in deionized water.

2.2. Raw materials characterisation

The elemental oxide composition was determined through X-ray fluorescence (XRF) analysis by a spectrophotometer Panalytical Philips PW 2400 sequential X-ray equipped with the software UniQuant® V5.0. The crystalline phases were identified using a PANalytical X'Pert PRO MPD alpha1 powder diffractometer device with CuKα_1 radiation. The SiO_2/Al_2O_3 availability was assessed by a chemical attack with NaOH solution to determine the reactive phases (SiO_2 and Al_2O_3) of CSP and PAVAL. The SiO_2/Al_2O_3 availability test consists of placing 1 g of powder raw materials in 100 mL 4 M, 6 M, and 8 M NaOH solutions, stirred constantly for 5 h in a sealed Teflon beaker at 80 °C [31]. The resulting solution was filtered and analysed by Perkin Elmer Optima ICP-OES 3200 RL equipment to quantify the Si and Al content. Leaching granular test (EN 12457-2) was carried out to determine the metal(loid)s concentration in CSP and PAVAL. The leachate analysis was conducted using an inductively coupled plasma mass spectrometry (ICP-MS) Perkin-Elmer Elan-6000 device.

2.3. Samples preparation

Table 1 summarises the mixture proportion of the AA-CSP/PV binders' formulations. Four different formulations were prepared by mixing CSP, PAVAL, and two NaOH solutions of 4 M and 6 M. The Si_2O/Al_2O_3 and Na_2O/Al_2O_3 ratios were set to specific values to enhance the mechanical performance and favour the alkali activation process, leading to different liquid-to-solid ratios. In this sense, the SiO_2/Al_2O_3 ratio was fixed at 2.0, maintaining the suitable CSP/PV proportion according to the selective chemical attacks to determine the available SiO_2 and Al_2O_3 depending on NaOH concentration. The value of the Si_2O/Al_2O_3 ratio allows for obtaining an optimal strength, as reported elsewhere [32]. The Na_2O/Al_2O_3 ratio was fixed at 1.2 and 1.5, considering the available Al_2O_3 and the amount of Na_2O in both NaOH solutions. The value of the Na_2O/Al_2O_3 ratio improves in the dissolution step of Si^{4+} and Al^{3+} and enhances the polymerization process [33].

The preparation of the AA-CSP/PV binders' formulations starts with an initial pre-treatment of PAVAL to remove the gas ammonia generated by the reaction of NaOH with the aluminium nitride in this aluminium residue [34]. This pre-treatment consists of stirring the alkali activator solutions (NaOH 4 M and NaOH 6 M) together with PAVAL for 24 h to
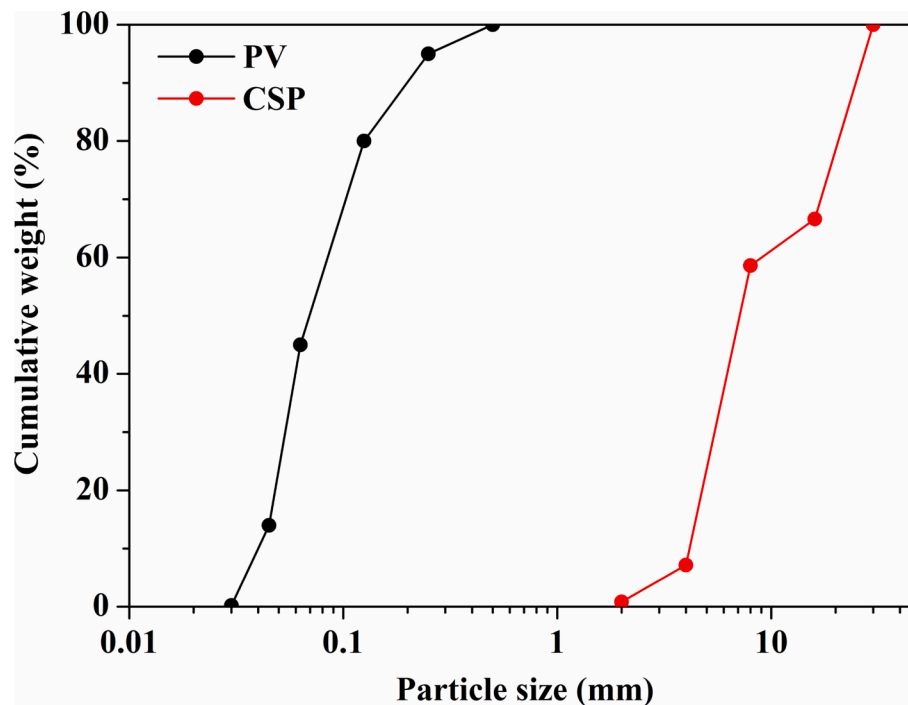
Fig. 1. Particle size distribution (PSD) of CSP and PAVAL®.

Table 1
AA-CSP/PV mix proportion.

Reference	S		L		SiO$_2$/Al$_2$O$_3$	Na$_2$O/Al$_2$O$_3$	L/S
	[1]CSP (wt. %)	[1]PV (wt. %)	[1]NaOH solution (wt. %)				
			4 M	6 M			
4M_1.2	73	27	72		2.0	1.2	0.72
4M_1.5	73	27	90		2.0	1.5	0.90
6M_1.2	70	30		51	2.0	1.2	0.51
6M_1.5	70	30		64	2.0	1.5	0.64

[1] wt.% respect to the total solid.

reduce the AA-CSP/PV binders' excessive porosity. The NaOH 8 M solution was discarded due to the extreme porosity generated during the curing of the specimens, which did not allow unmoulding of the samples after curing. After the pre-treatment, the powdered CSP is gradually added, mixed, and mechanically stirred with the NaOH with PAVAL solutions for 5 min at 760 rpm. The obtained pastes are poured into cubic moulds of 25-cubic-mm and sealed with a plastic bag. The decrease in liquid-to-solid ratios in the formulation of AA-CSP/PV binders decreased the fluidity of the fresh paste, and it was necessary to use a spatula to fill the moulds in the formulations made with NaOH 6 M. Then, the moulds are placed in an oven at 60 °C for 2 days. Finally, the samples are demoulded and cured at laboratory conditions (20 °C ± 1 °C and 50% ± 5% relative humidity) until to be tested.

2.4. Test methods

The analysis through x-ray diffraction and Fourier-transform infrared spectroscopy techniques and granular leaching test were conducted at different ages (3, 28, and 90 days) to assess the advancement of the gel formation attributable to alkali activation of the AA-CSP/PV binders (Table 2). The microstructure (SEM) and physicomechanical (bulk density, porosity, and compressive strength) characterisations were performed only at 28 days of curing.

2.4.1. Boiling water test

The hydrolytic stability of the AA-CSP/PV samples was assessed through the immersion of the specimens (previously dried in a desiccator with silica gel until constant weight) in boiling water for 20 min [35]. Afterwards, the specimens were placed in a desiccator with silica gel until constant weight. Finally, the specimens were weighed to determine the mass loss percentage and to certify the hydrolytic stability of all samples.

2.4.2. Physicochemical characterisation

X-ray diffraction (XRD) analysis was conducted using a PANalytical X'Pert PRO MPD alpha1 powder diffractometer device with CuKα$_1$ radiation to identify the main crystalline phases and reaction products in

Table 2
Characterisation methodology.

Characterisation type	Analysis technique/Test	Age (days)
Stability	Boiling water	28
Physicochemical	FT-IR	3, 28, 90
	XRD	3, 28, 90
	SEM	28
Physicomechanical	Apparent density	28
	Porosity	28
	Compressive strength	28
Environmental	Leaching test	14, 28, 90

AA-CSP/PV binders. Fourier-transformed infrared spectroscopy (FT-IR) in attenuated total reflectance mode (ATR) was performed using Spectrum Two™ equipment (Perkin Elmer) to assess the alkali activation process. The spectra of CSP and PAVAL and AA-CSP/PV binders were collected (32-scan average with 4 cm^{-1} resolution) and compared in the range 1500–500 cm^{-1} to evaluate the new formation and changes in the bands associated with (C,N)-A-S-H phases. The main band located around 950 cm^{-1}, which is attributed to the Si-O-Si or Si-O-Al bonds, was deconvoluted through Gaussian functions using OriginPro 2021 software as reported elsewhere [36]. The microstructure characterisation was performed by scanning electron microscopy-energy dispersive spectroscopy (SEM-EDS) analysis using ESEM FEI Quanta 200 equipment. The fractured specimens generated after the compressive strength were immersed in epoxy resin and then polished and coated with graphite due to the non-conductive nature of the samples.

2.4.3. Physical and mechanical properties

The bulk density and porosity were determined after 28 curing days. The bulk density was determined by measuring and weighing three cubic samples per formulation. The porosity was analysed through computer-based image analysis software (Image J™ 1.8.0). One sample per each formulation was cut in a half and 2D cross-section images were obtained by digital camera. The imported images were converted from RGB colour to 16-bit greyscale and the brightness/contrast and threshold tools were adjusted to differentiate between the pore and compact solid matrix (i.e. the number of pore pixels). The compressive strength (σ_c) tests after 3, 28 and 60 curing days were performed by Incotecnic MULTI-R1 equipment (loading rate of 240 kg·s^{-1} until fracture). Three measures per formulation were conducted.

2.4.4. Granular leaching test (EN 12457-2)

A granular leaching test (EN 12457-2) assessed the AA-CSP/PV binders' potential leaching metal(loid)s concentration. The alkaline activator solution increases pH during the preparation of the pastes, mobilising some pH-dependent heavy metal(loid)s. Therefore, a leaching test was performed in the powdered raw materials and crushed fragments (particles below 4 mm) of AA-CSP/PV binders. The powdered samples and fragments (two replicas per sample) were separately placed in plastic containers with deionised water (L/S ratio of 10 L·kg^{-1}) and then agitated (10 min^{-1}) for 24 h at room temperature. Then, one aliquot per sample was collected and filtered to analyse the heavy metal(loid)s concentration (As, Ba, Cd, Cr, Cu, Hg, Mo, Ni, Pb, Sb, Se, V, and Zn) through ICP-MS technique. Finally, the leaching metal(loid)s concentration was compared with the landfill acceptance limits established by EU legislation [37] to determine the hazardousness of AA-CSP/PV binders.

3. Results and discussion

3.1. Raw materials characterisation

The elemental oxide composition of CSP and PV is shown in Table 3. The results confirm that CSP and PAVAL can be used as silica and alumina source, respectively. Moreover, other essential oxides to formulate cementitious materials can be found in significant percentages in CSP (CaO, Al$_2$O$_3$, and Na$_2$O) and PAVAL (SiO$_2$, Na$_2$O, and MgO). However, it is important to indicate that these elements can be found in the form of different amorphous and crystalline phases, being the formers more reactive than the latter.

Although the CSP is mainly an amorphous material due to its high glass content, the XRD analysis revealed the presence of quartz (SiO$_2$; PDF# 01-079-1910) and mullite (Al$_{4.52}$Si$_{1.48}$O$_{9.74}$; PDF# 01-079-1457) as the main crystalline phases in CSP. In PAVAL, gibbsite (Al(OH)$_3$; PDF# 01-070-2038), nordstrandite (Al(OH)$_3$; PDF# 01-072-0623), bayerite (Al(OH)$_3$; PDF# 01-077-0114), corundum (Al$_2$O$_3$; PDF# 01-071-1123), and spinel (MgAl$_2$O$_4$; PDF# 01-077-0435) were identified as major crystalline phases. Aluminium nitride (AlN; PDF# 01-075-1620), potassium aluminium oxide (AlKO$_2$; PDF# 01-084-0380), potassium sodium aluminium silicate (Al(K,Na)O$_6$Si$_2$; PDF# 01-070-1260), calcium fluoride (CaF$_2$; PDF# 01-077-0245), cryolite (Na$_3$AlF$_6$; PDF# 25-0772), and quartz (SiO$_2$; PDF# 01-079-1910) were also detected as minor crystalline phases. The XRD results agree with the elemental composition shown in Fig. 2 since the main crystalline phases contain elements such as Si, Al, Mg, Ca, and Na.

The SiO$_2$ and Al$_2$O$_3$ availability of CSP and PAVAL determined by chemical attacks in NaOH 4 M and 6 M solutions is shown in Table 4. The potential of CSP and PAVAL as silica-rich and alumina-rich sources was demonstrated. However, the results revealed that significant parts of SiO$_2$ and Al$_2$O$_3$ in CSP and PAVAL are non-reactive probably due to their crystalline nature. It is important to highlight that SiO$_2$/Al$_2$O$_3$ and Na$_2$O/Al$_2$O$_3$ ratios were fixed considering the results obtained by chemical attacks for each molarity.

3.2. Boiling water test

The boiling water test demonstrated that the AA-CSP/PV binders were resistant to degradation in water. Although some insignificant defects were observed at the edges of the samples, the visual analysis revealed that all samples remained dimensionally unchanged. The percentage of weight loss (less than 1 wt% in all cases) also confirmed the hydrolytic stability of AA-CSP/PV binders, revealing the structural integrity of the samples due to the formation of new reaction products.

3.3. Physicochemical characterisation

The main crystalline phases in the formulations at 3, 28 and 90 days are summarised in Table 5. All the diffractograms present high amorphous content due to the unreacted CSP and (C,N)-A-S-H gels formed during the alkali activation process. The origin of most of the crystalline phases identified in the formulations comes mainly from PAVAL: corundum, silicon oxide (also detected in CSP), sodalite, magnesium aluminium oxide, calcium fluoride and aluminium oxide hydrate. Unlike the previously mentioned phases, aluminium oxide hydrate is not detected in the formulations at 28 and 90 days, probably due to the inclusion of Al in the AA-CSP/PV binders' structure. The new phases uniquely identified in the binders are katoite, zeolite P1, and sodium aluminium silicate hydrate. All the phases are sodium and calcium aluminosilicates, derived from the reaction in the formation of the cement, mainly because the activation process for AABs production is related to zeolite synthesis [38]. The influence of time was observed in the decrease of peak intensities and their disappearance at long times. This behaviour is detected predominantly in the zeolites P1 and sodium aluminium silicate hydrate. After 28 and 90 days of curing, the intensity of their peaks notably decreases. In some formulations, the phases were not detected, probably due to a collapse of the zeolite structure into an amorphous (C,N)-A-S-H gel. Trona and sodium hydrogen carbonate (both sodium carbonates) are also detected, especially at long times, which means that there is a carbonation process in the cement, probably
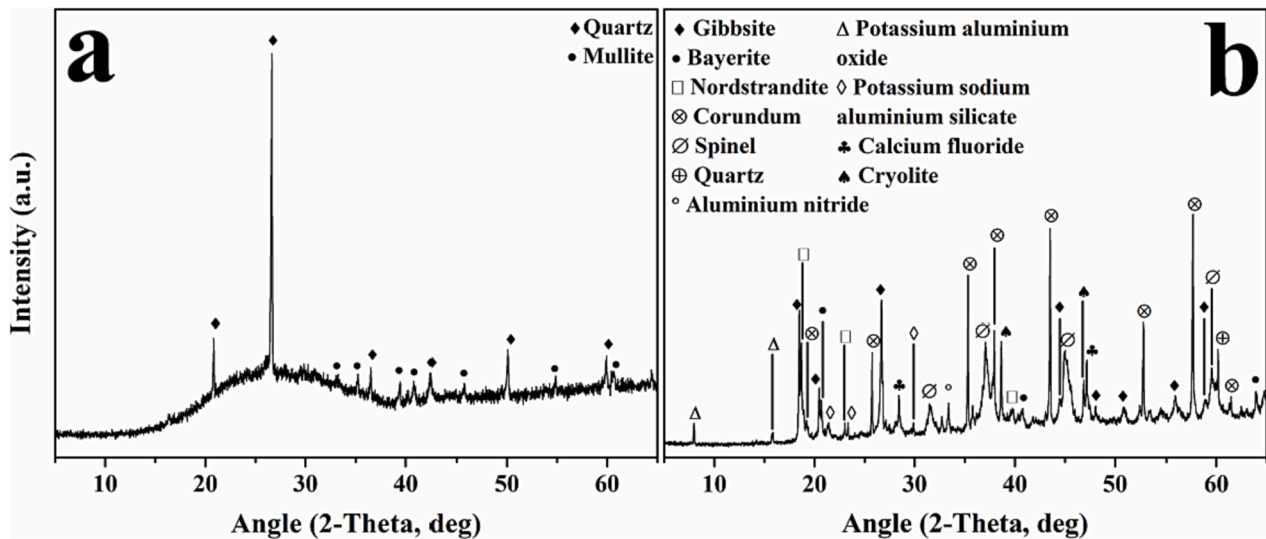
Table 3
Elemental composition of CSP and PAVAL.

Element (wt. %)	SiO$_2$	Al$_2$O$_3$	Na$_2$O	K$_2$O	Fe$_2$O$_3$	CaO	MgO	LOI
CSP	70.8	4.8	11.2	0.9	0.4	9.4	1.6	1.0
PAVAL	8.2	61.2	2.7	0.6	1.6	2.0	6.2	15.8

Fig. 2. XRD patterns of (a) CSP and (b) PAVAL.

Table 4
SiO$_2$ and Al$_2$O$_3$ availability of raw materials.

	4 M		6 M	
	SiO$_2$ (wt. %)	Al$_2$O$_3$ (wt. %)	SiO$_2$ (wt. %)	Al$_2$O$_3$ (wt. %)
CSP	16.1	0.8	16.2	0.8
PAVAL	2.5	36.5	5.1	34.2

due to the reaction of Na$^+$ from the alkaline activator with atmospheric CO$_2$ [39].

Fig. 3 depicts the FT-IR spectra of AA-CSP/PV binders after 3, 28, and 90 days of curing, focused on the mid-wavenumber region's broadband (1500–500 cm^{-1}) corresponding to Si-O-T bonds (T = Si, Al). The results revealed the variation in shape and position from the initial CSP broadband ($\approx$ 1000 cm^{-1}) compared to the band in the final binders' at 3 days. This initial broadband is narrowed and slightly shifted to lower wavenumbers in all cases due to the formation of new reaction products. From 3 to 28 days, there is a trend in the main band to shift to higher wavenumbers, probably due to the formation of (C,N)-A-S-H phases and the inclusion of Al in C-A-S-H gel [40]. Finally, from 28 to 90 days, there are no remarkable changes, only slight variations in formulations formulated with NaOH 6 M. This fact probably means that high molarity in the NaOH flatters and lengthens the alkali activation process.

To conduct a more comprehensive analysis of the IR results, the deconvolution of the main band of the IR spectra into four peaks for each formulation and time was also performed, while ensuring a minimum adjusted R^2 of 0.999. The variation of the deconvoluted peaks can be observed in Fig. 4. In a general sense, the most pronounced variations and changes are observed in the 3 to 28 days' time period. In contrast, from 28 to 90 days, there is less variation from the bands. This fact revealed that the alkali activation process occurs predominantly in the first 28 days, and subsequently, there is only a small reaction of some unreacted precursors. The peaks that present higher variation with time

Table 5
Crystalline phases of AA-CSP/PV binders at 3, 28, and 90 days.

| Crystalline phase	PDF	Formulation											
		3 days				28 days				90 days			
		4M-1.2	4M-1.5	6M-1.2	6M-1.5	4M-1.2	4M-1.5	6M-1.2	6M-1.5	4M-1.2	4M-1.5	6M-1.2	6M-1.5
Corundum	01-071-1123	✓	✓	✓	✓	✓	✓	✓	✓	✓	✓	✓	✓
Silicon Oxide	01-085-0695	✓	✓	✓	✓	✓	✓	✓	✓	✓	✓	✓	✓
Sodalite	01-086-1030	✓	✓	✓	✓	✓	✓	✓	✓	✓	✓	✓	✓
Magnesium Aluminium Oxide	01-074-1133	✓	✓	✓	✓	✓	✓	✓	✓	✓	✓	✓	✓
Calcium Fluoride	01-075-0363	✓	✓	✓	✓	✓	✓	✓	✓	✓	✓	✓	✓
Katoite	01-077-1713	✓	✓	✓	✓	✓	✓	✓	✓	✓	✓	✓	✓
Zeolite P1	01-071-0962	✓	✓	✓	✓	✓	✓	✓	✓	✓	✓	–	–
Sodium Aluminium Silicate Hydrate	00-038-0241	✓	✓	✓	✓	✓	✓	✓	✓	✓	✓	–	–
Sodium Hydrogen Carbonate	01-074-1203	–	–	–	–	✓	✓	✓	✓	✓	✓	✓	✓
Trona	01-078-1064	–	–	✓	–	✓	✓	✓	✓	–	–	–	–
Aluminium Oxide Hydrate	01-070-0384	✓	–	✓		–	–	–	–	–	–	–	–
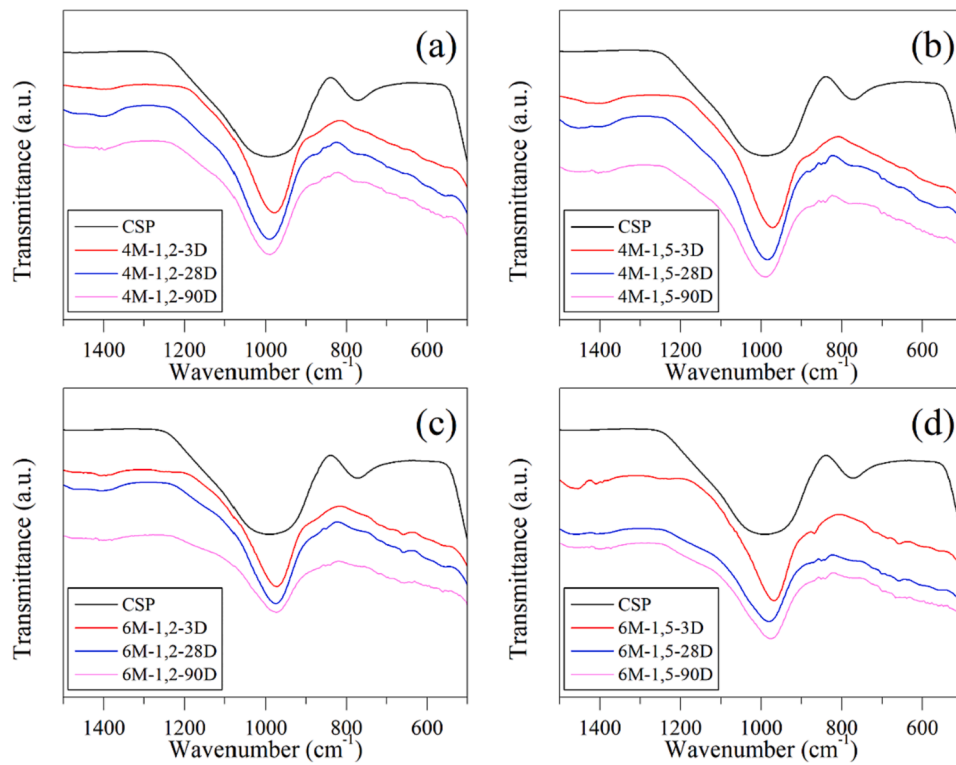
Fig. 3. FT-IR spectra of AA-CSP/PV binders at 3, 28, and 90 days of curing: (a) 4M-1,2 (b) 4M-1,5 (c) 6M-1,2 (d) 6M-1,5.
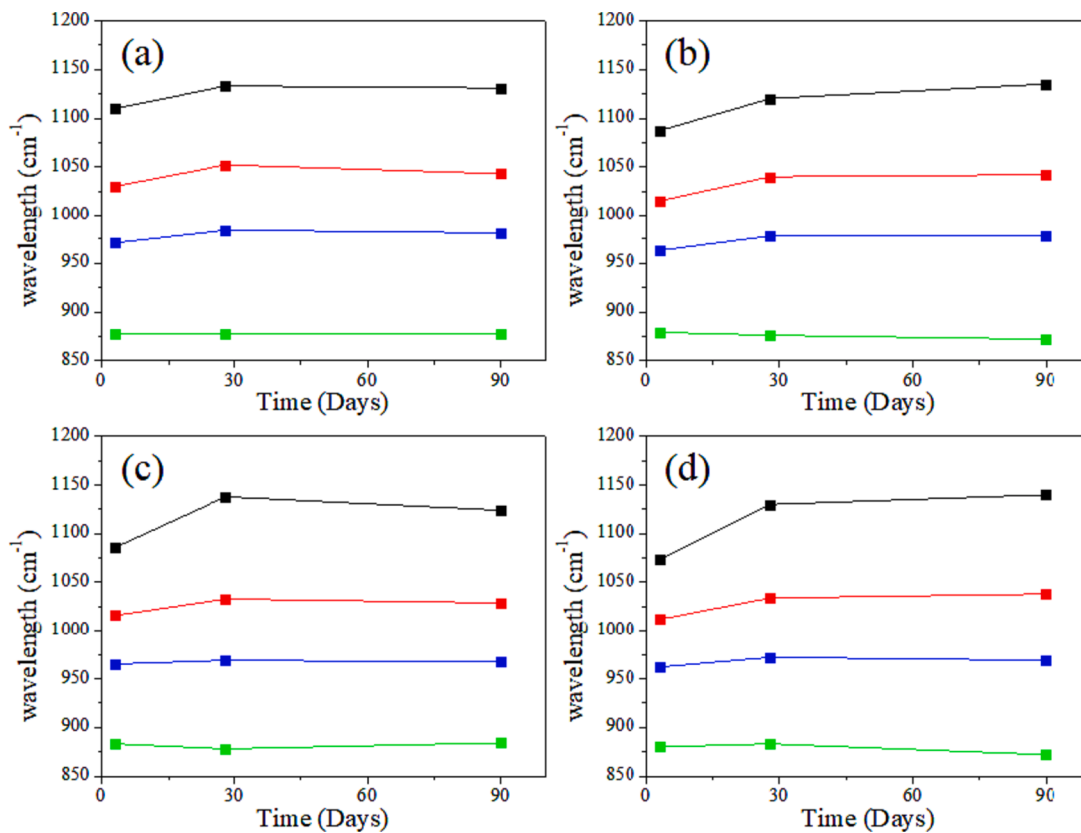

Fig. 4. Variation of deconvoluted peaks wavelengths of (a) 4M-1,2 (b) 4M-1,5 (c) 6M-1,2 (d) 6M-1,5 formulations over time.

are those of the highest wavenumber (~1070–1140 and ~1010–1050), assigned to Si-O-Si stretching bond and Si-O-Al stretching, respectively. This change is probably due to the inclusion of Al in the gel structure. The difference between formulations is due to the variation of precursor relative amount (more or less Al reacting). The peak assigned to Si-O-Al (~970 cm^{-1}) presents less variation with time and small variation with formulations, probably due to the different amounts of Al (from PAVAL) used in the AA-CSP/PV binders' formulation. The band at ~880 cm^{-1}, assigned to Si-O terminal bonds, remains constant with formulation and time, as the Al inclusion in the structure does not affect it. Furthermore, there is a reduction in the relative area of this band from 3 to 28 days, together with an increase of Si-O-Si and Si-O-Al bands areas, meaning that some of the Si-O terminal bonds probably react with Al or Si due to the alkali activation process.

Fig. 5 depicts the AA-CSP/PV binders' micrographs in backscattering electron (BSE) mode and the EDS spectra collected in different zones (matrix and particles) of the samples. The matrix EDS spectrum revealed the formation of (C,N)-A-S-H gels due to the prominent presence of Si, Al, Ca, and Na elements, which agrees with the previous XRD and FT-IR results. The existence of microcracks can also be observed in all samples, mainly in the 6M-1.2 sample, which presented the more compact matrix. Furthermore, the micrographs showed a generalised presence of unreacted particles in all samples. These particles can be attributed to CSP or PAVAL particles due to the presence of Si, Na, and Ca (see CSP particles EDS spectrum) or Al (see PAVAL particles EDS spectrum), essential elements for glass or aluminium manufacturing. On the other hand, a significant difference in the samples' porosity can also be observed, which is thoroughly examined in the next section.

3.4. Physical and mechanical properties

The bulk density, porosity, and compressive strength of AA-CSP/PV binders at 28 days of curing are shown in Fig. 6. The results were consistent for all samples since the density and compressive strength results showed an inverse trend to porosity. The formulations activated with NaOH 6 M had a lower porosity than those made with NaOH 4 M due to the significant difference between the L/S ratio in the formulations activated with NaOH 4 M (0.72 and 0.9) and NaOH 6 M (0.51 and 0.64). The formulations activated with the same molarity and Na$_2$O/Al$_2$O$_3$ ratio (1.2 vs 1.5) revealed a higher porosity when the amount of NaOH increased since their higher L/S ratio (0.9 and 0.64) favours the evaporation during the curing process, increasing the porosity of the samples. The 6M_1.2 sample, which had the highest density (1.3 g·cm^{-3}), showed the best mechanical performance (18.2 MPa), as expected. Therefore, it could be used for non-structural building and civil engineering purposes. On the other hand, the remaining samples revealed a low density (below 0.8 g·cm^{-3}) and mechanical performance (below 5 MPa), which limit their application as lightweight or thermal insulation material.

Despite the consistency in the results of bulk density, porosity, and compressive strength, the difference in mechanical performance between the 4M-1.5 (2.9 MPa) sample with the 4M_1.2 (5.3 MPa) and 6M-1.5 (5.9 MPa) samples was unexpected if we consider their porosity (48%, 37%, and 35%, respectively). This difference can be explained through the pore shape and distribution, as seen in Fig. 7. The 4M_1.5 sample (Fig. 7b) presented a homogeneous porosity with well-distributed spherical or oval-shaped pores. However, the 4M_1.2 (Fig. 7a) and 6M_1.5 (Fig. 7d) samples showed heterogeneous undistributed and interconnected pores with different sizes and shapes, which contributes to a significant decrease in their mechanical performance
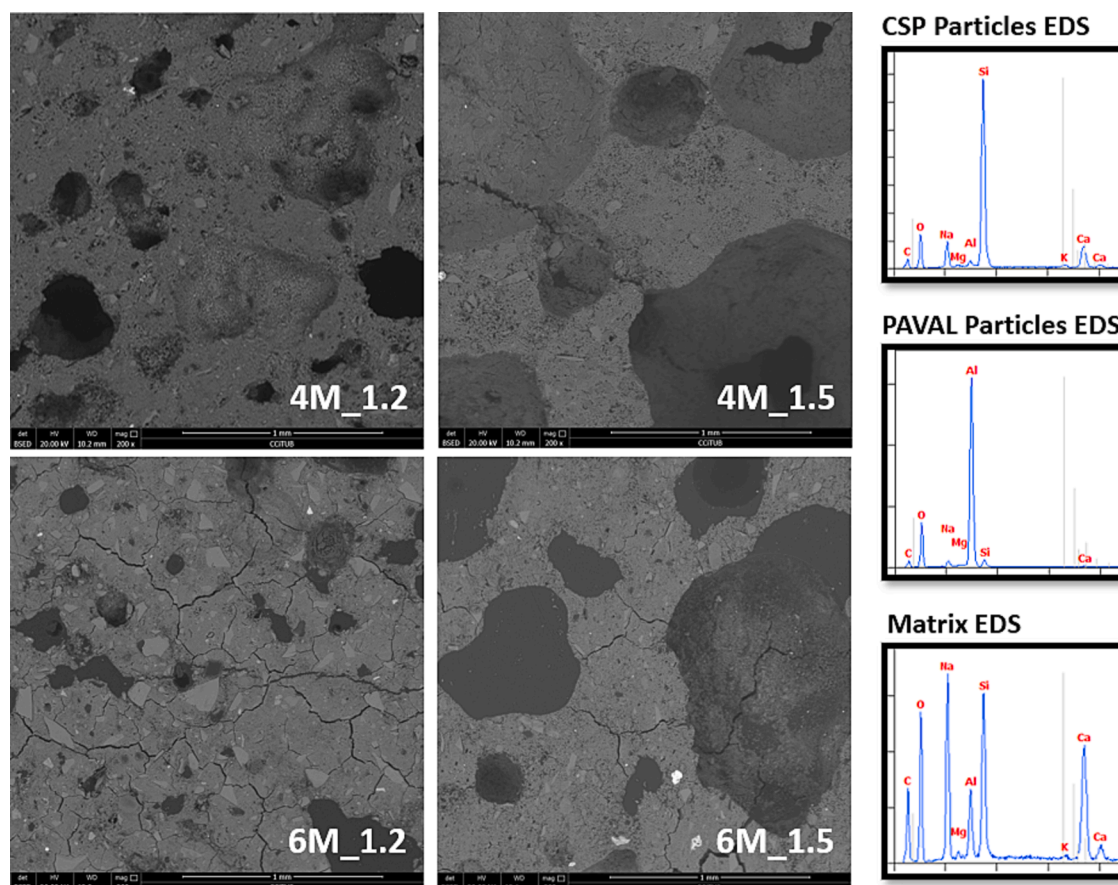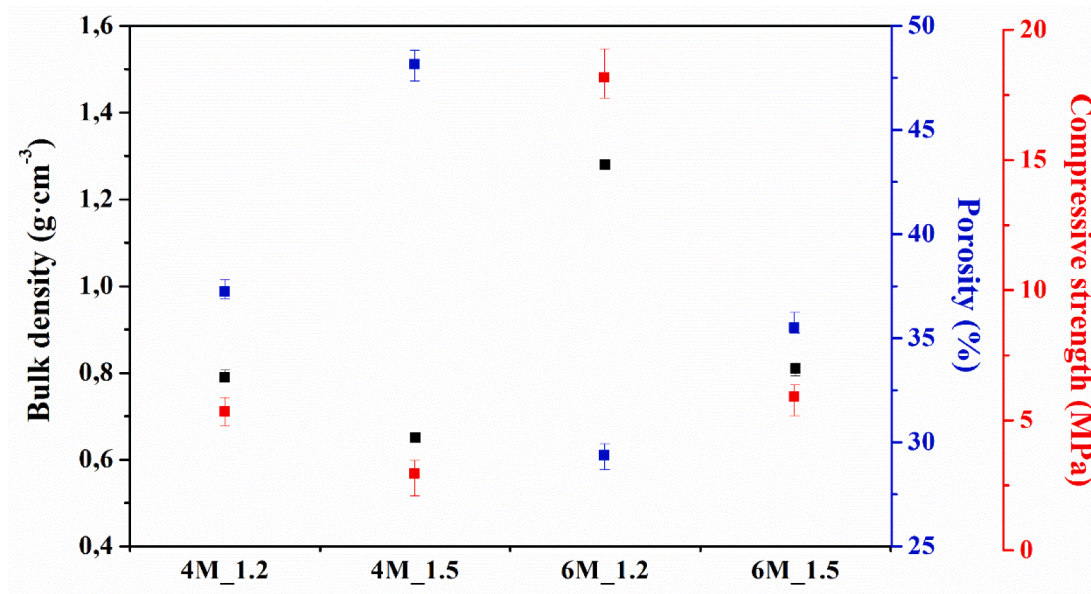

Fig. 5. SEM micrographs of AA-CSP/PV binders.

Fig. 6. Bulk density, porosity, and compressive strength of AA-CSP/PV binders at 28 days of curing.
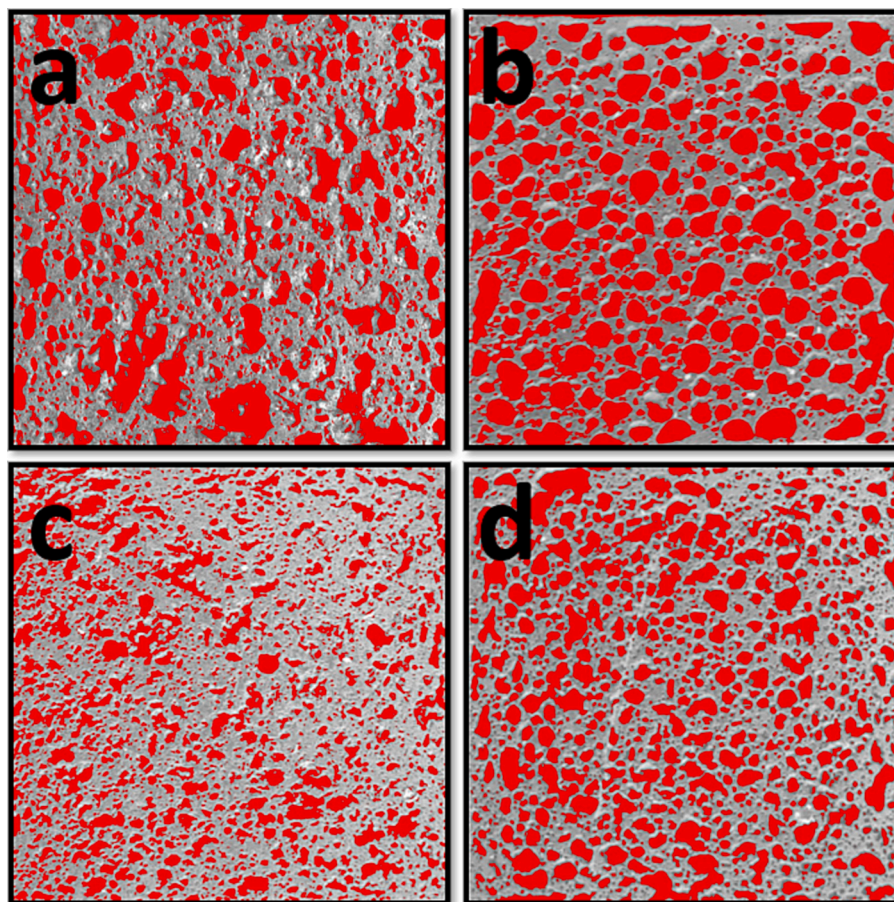

Fig. 7. Porosity determination of AA-CSP/PV binders obtained from ImageJ: (a) 4M_1.2 (b) 4M_1.5 (c) 6M_1.2 (d) 6M-1.5.

[41,42]. Finally, the porosity of the 6M-1.2 sample (Fig. 7c) was around 29 %; despite its heterogeneous porosity, the generalised small pore size contributed to the enhancement of compressive strength compared with the other samples.

3.5. Granular leaching test (EN 12457-2)

The potential release of heavy metal(loid)s in CSP, PAVAL, and AA-CSP/PV binders (14, 28, and 90 days) was evaluated through a granular leaching test (EN 12457-2). This test's main goal was to compare raw

Table 6
Leaching concentrations (mg·kg^{-1}) in raw materials and AA-CSP/PV binders after leaching granular test (EN 12457–2).

Sample	As	Ba	Cd	Cr	Cu	Hg	Mo	Ni	Pb	Sb	Se	Zn
Raw materials												
CSP	0.65	0.72	<0.01	0.06	0.74	<0.01	0.02	0.07	0.01	0.37	0.20	0.17
PAVAL	0.10	0.06	<0.01	0.01	0.15	<0.01	2.90	<0.20	0.01	1.38	<0.10	0.10
AA-CSP/PV binders												
14 days												
4M-1.2	26.35	0.29	0.00	0.17	0.55	0.01	4.49	0.05	0.02	3.98	1.58	0.07
4M-1.5	24.68	0.39	0.01	0.33	0.86	0.01	4.59	0.08	0.03	4.70	1.61	0.18
6M-1.2	22.10	0.24	0.01	0.18	0.87	0.01	4.84	0.14	0.04	6.48	1.35	0.14
6M-1.5	21.47	0.60	0.01	0.13	1.04	0.01	5.50	0.09	0.03	4.15	1.39	0.15
28 days												
4M-1.2	20.09	0.28	0.01	0.14	0.44	0.01	3.79	0.03	0.01	2.36	1.37	0.11
4M-1.5	18.52	0.33	0.01	0.26	0.49	0.003	4.10	0.04	0.01	2.49	1.51	0.17
6M-1.2	17.32	0.25	0.01	0.07	0.74	0.004	4.44	0.07	0.02	3.02	1.18	0.31
6M-1.5	17.20	0.54	0.01	0.15	0.57	0.002	4.82	0.05	0.01	2.03	1.33	0.12
90 days												
4M-1.2	21.01	0.25	<0.01	1.01	0.57	<0.02	4.01	0.03	0.02	1.23	0.88	<0.40
4M-1.5	19.41	0.62	<0.01	1.61	0.56	<0.02	3.81	0.03	0.01	1.11	0.85	<0.40
6M-1.2	15.52	0.25	<0.01	0.28	0.43	<0.02	4.02	0.05	0.01	1.19	0.53	<0.40
6M-1.5	17.73	0.89	<0.01	1.21	0.59	<0.02	5.03	0.02	0.04	0.93	0.62	<0.40
[1]Inert waste (mg·kg^{-1})	0.5	20	0.04	0.5	2	0.01	0.5	0.4	0.5	0.06	0.1	4
[1]Non-hazardous waste (mg·kg^{-1})	2	100	1	10	50	0.2	10	10	10	0.7	0.5	50
[1]Hazardous waste (mg·kg^{-1})	25	300	5	70	100	2	30	40	50	5	7	200

[1] Limit for waste acceptance in landfills [37].

materials' initial hazardousness with the AA-CSP/PV binders since alkali activation increases the alkalinity of the medium, leading to an increase in pH-dependents metal(loid)s concentration [31]. Table 6 summarises the leaching concentration of 12 metal(loid)s in deionised water and the leaching limit values for its acceptance in landfills [37]. CSP could be classified as non-hazardous waste since the As, Sb, and Se limits exceed the inert waste limit. As and Sb are used in the glass industry as clarifying and (de)colouring agents in the form of oxides (As_2O_3 and Sb_2O_3). PAVAL would be classified as hazardous waste because the Sb concentration exceeds the non-hazardous waste limit. The antimony's presence in PAVAL is due to this element's use in some aluminium-bearing alloys

containing at least 4–6% of Sb [43].

Regarding the leaching concentrations in AA-CSP/PV binders, the results revealed a severe activation in some metal(loid)s (As, Cr, Mo, Sb, and Se) due to the high alkalinity of NaOH solutions used as alkaline activators. Therefore, considering this granular leaching test as the end-of-life scenario, AA-CSP/PV binders should be classified as hazardous waste since As, Sb, and Se exceeded the non-hazardous threshold classification. However, Fig. 8 shows a generalised downward trend in the leaching concentration of the above-mentioned metal(loid)s, except for the Cr, revealing a probable enhancement of the encapsulation effect with long curing time [44].
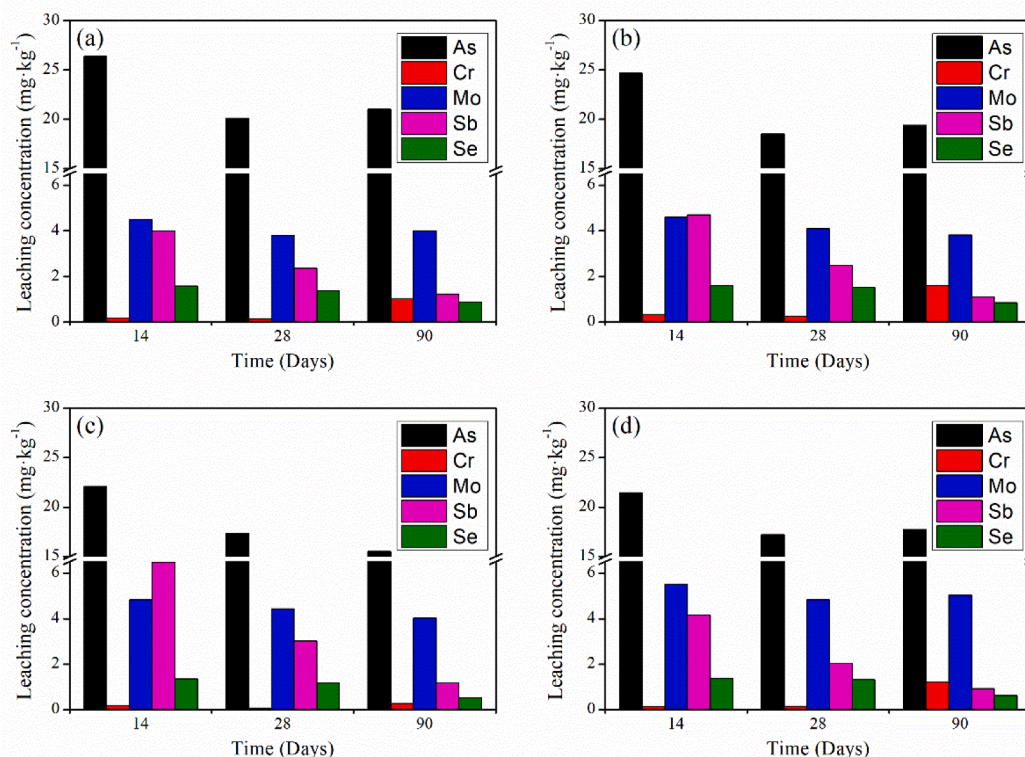

Fig. 8. Evolution of leaching concentration of As, Cr, Mo, Sb, and Se at 14, 28, and 90 days of curing: (a) 4M-1.2 (b) 4M-1.5 (c) 6M-1.2 (d) 6M-1.5.

4. Conclusions

This research demonstrates the potential of CSP and PAVAL as precursors in alkali activation technology and promotes sustainability criteria such as the reduction of natural resources extraction activity or the low carbon footprint materials manufacturing.

CSP and PAVAL are generated during the glass and aluminium recycling processes and contain a significant amount of reactive silica and alumina, as revealed in their chemical characterisation. Furthermore, the combination of both precursors, as silica and alumina sources, with different NaOH solutions (4 M and 6 M) as the alkaline activators allowed the development of high-porosity alkali-activated binders (AA-CSP/PV binders).

The FT-IR spectra of AA-CSP/PV binders showed the displacement of Si-O-T bonds (T = Si, Al) throughout time, indicating the alkali activation of CSP and PAVAL. Furthermore, detecting crystalline phases such as zeolite P1, katoite, and sodium aluminium silicate hydrate in AA-CSP/PV binders demonstrated the formation of (C,N)-A-S-H gels. These results were also consistent with the EDS analysis since the cementitious matrix spectra showed the simultaneous presence of Si, Al, Na, and Ca. On the other hand, despite carrying out a PAVAL pretreatment to remove the gas ammonia generated by the reaction of NaOH and aluminium nitride, the physicomechanical characterisation revealed the high porosity of AA-CSP/PV binders, making them well-suited for use in thermal and acoustic insulation or non-structural purposes. Finally, the environmental characterisation demonstrated the severe activation of some heavy metal(loid)s such as As, Sb, and Se. However, the encapsulation efficiency of these metal(loid)s improves over time.

Future line research should focus on controlling and monitoring the pore size, shape, and distribution generated by PAVAL by using additives such as surfactants since reaching a homogeneous porosity would improve the mechanical performance of the AA-CSP/PV binders. In addition, thermal and acoustic characterisation should be evaluated to determine the potential of AA-CSP/PV binders as insulation construction materials.

Declaration of Competing Interest

The authors declare that they have no known competing financial interests or personal relationships that could have appeared to influence the work reported in this paper.

Data availability

Data will be made available on request.

References

[1] Y.C. Wong, S. Perera, Z. Zhang, A. Arulrajah, A. Mohammadinia, Field study on concrete footpath with recycled plastic and crushed glass as filler materials, Constr. Build. Mater. 243 (2020), 118277, https://doi.org/10.1016/j.conbuildmat.2020.118277.

[2] A. Mehta, D.K. Ashish, Silica fume and waste glass in cement concrete production: A review, J. Build. Eng. 29 (2020), 100888, https://doi.org/10.1016/j.jobe.2019.100888.

[3] P. Guo, W. Meng, H. Nassif, H. Gou, Y. Bao, New perspectives on recycling waste glass in manufacturing concrete for sustainable civil infrastructure, Constr. Build. Mater. 257 (2020), 119579, https://doi.org/10.1016/j.conbuildmat.2020.119579.

[4] A.B. Pascual, M.T. Tognonvi, A. Tagnit-hamou, Waste glass powder-based alkali-activated mortar, (2014) 32–36.

[5] Y. Jiang, T.C. Ling, K.H. Mo, C. Shi, A critical review of waste glass powder – Multiple roles of utilization in cement-based materials and construction products, J. Environ. Manage. 242 (2019) 440–449, https://doi.org/10.1016/j.jenvman.2019.04.098.

[6] E.T. Bueno, J.M. Paris, K.A. Clavier, C. Spreadbury, C.C. Ferraro, T.G. Townsend, A review of ground waste glass as a supplementary cementitious material: A focus on alkali-silica reaction, J. Clean. Prod. 257 (2020), 120180, https://doi.org/10.1016/j.jclepro.2020.120180.

[7] F. Andreola, L. Barbieri, I. Lancellotti, C. Leonelli, T. Manfredini, Recycling of industrial wastes in ceramic manufacturing: state of art and glass case studies, Ceram. Int. 42 (2016) 13333–13338, https://doi.org/10.1016/j.ceramint.2016.05.205.

[8] R. Xiao, Y. Ma, X. Jiang, M. Zhang, Y. Zhang, Y. Wang, B. Huang, Q. He, Strength, microstructure, efflorescence behavior and environmental impacts of waste glass geopolymers cured at ambient temperature, J. Clean. Prod. 252 (2020), 119610, https://doi.org/10.1016/j.jclepro.2019.119610.

[9] C. Ma, B. Zhao, S. Guo, G. Long, Y. Xie, Properties and characterization of green one-part geopolymer activated by composite activators, J. Clean. Prod. 220 (2019) 188–199, https://doi.org/10.1016/j.jclepro.2019.02.159.

[10] M.B. Ali, R. Saidur, M.S. Hossain, A review on emission analysis in cement industries, Renew. Sustain. Energy Rev. 15 (2011) 2252–2261, https://doi.org/10.1016/j.rser.2011.02.014.

[11] Y. Zhang, R. Xiao, X. Jiang, W. Li, X. Zhu, B. Huang, Effect of particle size and curing temperature on mechanical and microstructural properties of waste glass-slag-based and waste glass-fly ash-based geopolymers, J. Clean. Prod. 273 (2020), 122970, https://doi.org/10.1016/j.jclepro.2020.122970.

[12] W. Hu, Q. Nie, B. Huang, X. Shu, Q. He, Mechanical and microstructural characterization of geopolymers derived from red mud and fly ashes, J. Clean. Prod. 186 (2018) 799–806, https://doi.org/10.1016/j.jclepro.2018.03.086.

[13] M. Vukčević, D. Turović, M. Krgović, I. Bošković, M. Ivanović, R. Zejak, Utilization of geopolymerization for obtaining construction materials based on red mud, Mater. Tehnol. 47 (2013) 99–104.

[14] P. Sturm, G.J.G. Gluth, H.J.H. Brouwers, H.C. Kühne, Synthesizing one-part geopolymers from rice husk ash, Constr. Build. Mater. 124 (2016) 961–966, https://doi.org/10.1016/j.conbuildmat.2016.08.017.

[15] E. Najafi Kani, A. Allahverdi, J.L. Provis, Efflorescence control in geopolymer binders based on natural pozzolan, Cem. Concr. Compos. 34 (2012) 25–33, https://doi.org/10.1016/j.cemconcomp.2011.07.007.

[16] H. Doweidar, Y.M. Moustafa, S.A. El-maksoud, H. Silim, Properties of Na 2 O – Al 2 O 3 – B 2 O 3 glasses, 301 (2001) 207–212.

[17] R. Xiao, Y. Zhang, X. Jiang, P. Polaczyk, Y. Ma, B. Huang, Alkali-activated slag supplemented with waste glass powder: Laboratory characterization, thermodynamic modelling and sustainability analysis, J. Clean. Prod. 286 (2021), 125554, https://doi.org/10.1016/j.jclepro.2020.125554.

[18] M. Vafaei, A. Allahverdi, High strength geopolymer binder based on waste-glass powder, Adv. Powder Technol. 28 (2017) 215–222, https://doi.org/10.1016/j.apt.2016.09.034.

[19] F. Puertas, M. Torres-Carrasco, Use of glass waste as an activator in the preparation of alkali-activated slag. Mechanical strength and paste characterisation, Cem. Concr. Res. 57 (2014) 95–104, https://doi.org/10.1016/j.cemconres.2013.12.005.

[20] H.K. Tchakouté, C.H. Rüscher, S. Kong, E. Kamseu, C. Leonelli, Geopolymer binders from metakaolin using sodium waterglass from waste glass and rice husk ash as alternative activators: A comparative study, Constr. Build. Mater. 114 (2016) 276–289, https://doi.org/10.1016/j.conbuildmat.2016.03.184.

[21] M. Torres-Carrasco, F. Puertas, Waste glass in the geopolymer preparation. Mechanical and microstructural characterisation, J. Clean. Prod. 90 (2015) 397–408, https://doi.org/10.1016/j.jclepro.2014.11.074.

[22] B.C. Bunker, G.W. Arnold, E.K. Beauchamp, D.E. Day, Mechanisms for alkali leaching in mized-NaK silicate glasses, J. Non. Cryst. Solids. 58 (1983) 295–322, https://doi.org/10.1016/0022-3093(83)90031-5.

[23] R. Redden, N. Neithalath, Microstructure, strength, and moisture stability of alkali activated glass powder-based binders, Cem. Concr. Compos. 45 (2014) 46–56, https://doi.org/10.1016/j.cemconcomp.2013.09.011.

[24] X. Gao, X. Yao, R. Xie, X. Li, J. Cheng, T. Yang, Performance of fly ash-based geopolymer mortars with waste cathode ray tubes glass fine aggregate: A comparative study with cement mortars, Constr. Build. Mater. 344 (2022), 128243, https://doi.org/10.1016/j.conbuildmat.2022.128243.

[25] N. Toniolo, A. Rincón, Y.S. Avadhut, M. Hartmann, E. Bernardo, A.R. Boccaccini, Novel geopolymers incorporating red mud and waste glass cullet, Mater. Lett. 219 (2018) 152–154, https://doi.org/10.1016/j.matlet.2018.02.061.

[26] J. Giro-Paloma, A. Maldonado-Alameda, A. Alfocea-Roig, J. Mañosa, J. M. Chimenos, J. Formosa, Preliminary study of new sustainable, alkali-activated

cements using the residual fraction of the glass cullet recycling as precursor, Appl. Sci. 11 (8) (2021) 3528.

[27] C. García Serrada, J. del Cerro Iglesias, Utilización de Paval como filler de aportación para la fabricación de mezclas bituminosas en caliente, Carreteras Rev. Técnica La Asoc. Española La Carret. 123 (2002) 81–92.

[28] A. Font, L. Soriano, J. Monzó, J.C.B. Moraes, M.V. Borrachero, J. Payá, Salt slag recycled by-products in high insulation alternative environmentally friendly cellular concrete manufacturing, Constr. Build. Mater. 231 (2020), 117114, https://doi.org/10.1016/j.conbuildmat.2019.117114.

[29] C. Leiva, Y. Luna-Galiano, C. Arenas, B. Alonso-Fariñas, C. Fernández-Pereira, A porous geopolymer based on aluminum-waste with acoustic properties, Waste Manag. 95 (2019) 504–512, https://doi.org/10.1016/j.wasman.2019.06.042.

[30] A. Maldonado-Alameda, J. Mañosa, J. Giro-Paloma, J. Formosa, J.M. Chimenos, Synthesis of alkali-activated binders based on waste-to-energy bottom ash and aluminium recycling waste, J. Build. Eng. under revi (2020).

[31] A. Maldonado-Alameda, J. Giro-Paloma, A. Svobodova-Sedlackova, J. Formosa, J. M. Chimenos, Municipal solid waste incineration bottom ash as alkali-activated cement precursor depending on particle size, J. Clean. Prod. 242 (2020) 1–10, https://doi.org/10.1016/j.jclepro.2019.118443.

[32] C. Ruiz-Santaquiteria, J. Skibsted, A. Fernández-Jiménez, A. Palomo, Alkaline solution/binder ratio as a determining factor in the alkaline activation of aluminosilicates, Cem. Concr. Res. 42 (2012) 1242–1251, https://doi.org/10.1016/j.cemconres.2012.05.019.

[33] A. Maldonado-Alameda, J. Giro-Paloma, F. Andreola, L. Barbieri, J.M. Chimenos, I. Lancellotti, Weathered bottom ash from municipal solid waste incineration: Alkaline activation for sustainable binders, Constr. Build. Mater. 327 (2022), 126983, https://doi.org/10.1016/j.conbuildmat.2022.126983.

[34] D. Bajare, G. Bumanis, A. Korjakins, New porous material made from industrial and municipal waste for building application, Mater. Sci. 20 (2014) 3–8, https://doi.org/10.5755/j01.ms.20.3.4330.

[35] À. Maldonado-Alameda, J. Giro-Paloma, A. Alfocea-Roig, J. Formosa, J. M. Chimenos, Municipal solid waste incineration bottom ash as sole precursor in the alkali-activated binder formulation, Appl. Sci. 10 (2020) 1–15, https://doi.org/10.3390/app10124129.

[36] J. Mañosa, A.M. Gómez-Carrera, A. Svobodova-Sedlackova, A. Maldonado-Alameda, A. Fernández-Jiménez, J.M. Chimenos, Potential reactivity assessment of mechanically activated kaolin as alternative cement precursor, Appl. Clay Sci. 228 (2022) 106648.

[37] Council of the European Union, Council Decision establishing criteria and procedures for the acceptance of waste at landfills pursuant to Article 16 of and Annex II to Directive 1999/31/EC, European Union, 2003.

[38] S.A. Bernal, J.L. Provis, V. Rose, R.M. de Gutiérrez, J. Biernacki, High-resolution X-ray diffraction and fluorescence microscopy characterization of alkali-activated slag-metakaolin binders, J. Am. Ceram. Soc. 96 (6) (2013) 1951–1957.

[39] R. Occhipinti, A. Stroscio, C. Finocchiaro, M. Fugazzotto, C. Leonelli, M. José Lo Faro, B. Megna, G. Barone, P. Mazzoleni, Alkali activated materials using pumice from the Aeolian Islands (Sicily, Italy) and their potentiality for cultural heritage applications: preliminary study, Constr. Build. Mater. 259 (2020), 120391, https://doi.org/10.1016/j.conbuildmat.2020.120391.

[40] B. Walkley, R. San Nicolas, M.A. Sani, G.J. Rees, J.V. Hanna, J.S.J. van Deventer, J. L. Provis, Phase evolution of C-(N)-A-S-H/N-A-S-H gel blends investigated via alkali-activation of synthetic calcium aluminosilicate precursors, Cem. Concr. Res. 89 (2016) 120–135, https://doi.org/10.1016/j.cemconres.2016.08.010.

[41] K. Lyu, W. She, C. Miao, H. Chang, Y. Gu, Quantitative characterization of pore morphology in hardened cement paste via SEM-BSE image analysis, Constr. Build. Mater. 202 (2019) 589–602, https://doi.org/10.1016/j.conbuildmat.2019.01.055.

[42] Y. Su, J. Zhu, X. Long, L. Zhao, C. Chen, C. Liu, Statistical effects of pore features on mechanical properties and fracture behaviors of heterogeneous random porous materials by phase-field modeling, Int. J. Solids Struct. 264 (2023), 112098, https://doi.org/10.1016/j.ijsolstr.2022.112098.

[43] A. Maldonado-Alameda, J. Giro-Paloma, A. Rodríguez-Romero, J. Serret, A. Menargues, A. Andrés, J.M. Chimenos, Environmental potential assessment of MSWI bottom ash-based alkali-activated binders, J. Hazard. Mater. 416 (2021) 125828.

[44] I. Lancellotti, M. Catauro, F. Dal, J. Kiventer, C. Leonelli, M. Illikainen, Alkali activation as new option for gold mine tailings inertization, J. Clean. Prod. 187 (2018) 76–84, https://doi.org/10.1016/j.jclepro.2018.03.182.